Dalton Transactions

ROYAL SOCIETY OF CHEMISTRY

PAPER

View Article Online
View Journal

Cite this: DOI: 10.1039/d0dt02069a

Hypoxia efficient and glutathione-resistant cytoselective ruthenium(II)-*p*-cymene-arylimidazophenanthroline complexes: biomolecular interaction and live cell imaging†

Ashaparna Mondal and Priyankar Paira *

Received 10th June 2020,
Accepted 11th August 2020

DOI: 10.1039/d0dt02069a

rsc.li/dalton

Due to the side effects of marketed cancer drugs, we designed a series of ruthenium-based fluorescent anticancer drugs, which was demonstrated to be target specific, highly cytoselective, lipophilic, water soluble, hypoxia efficient and glutathione resistant. Herein, we developed novel ruthenium(II)-*p*-cymene-2-aryl-imidazophenanthroline scaffolds as effective DNA-targeting agents. Specifically, the 2-aryl substituted imidazophenanthroline ligands make the Ru(II) complex a decent DNA intercalator by affording planarity. Among the four Ru(II) complexes (**RuL1–RuL4**), [(η^6-*p*-cymene)Ru^{II}Cl{K^2-*N*,*N*-(2-(naphthalene-1-yl)-1*H*-imidazo[4,5-*f*][1,10]phenanthroline)}]PF_6 (**RuL4**) exhibited the best cytoselectivity in two cancer cell lines (Caco-2 and HeLa), and [(η^6-*p*-Cymene)Ru^{II}Cl{K^2-*N*,*N*-(2-(anthracen-9-yl)-1*H*-imidazo[4,5-*f*][1,10]phenanthroline)}]PF_6 (**RuL1**) was established as a potent HeLa cell imaging probe.

Introduction

Cancer is defined as the uncontrolled proliferation of abnormal cells in the body.[1] Metallotherapeutics can play a vital role in inhibiting the division of cancer cells, and consequently trigger cancer cell apoptosis, inducing DNA damage and disrupting DNA repair progression.[2–4] The extensively used structurally similar platinum-based drugs, *i.e.*, cisplatin, carboplatin and oxaliplatin, have achieved pronounced success for cancer therapy worldwide.[5] However, the emergence of platinum resistance and considerable side effects have strongly restricted their therapeutic importance in clinical use, and thus led researchers to explore non-platinum metal complexes for anti-cancer drug discovery.[6–13] In our current drug discovery research, a ruthenium(II) complex has been highlighted as a cytoselective and cost-effective drug with respect to platinum, and its mechanism of action has already been discussed.[14] In the past few decades, ruthenium complexes have effectively been used in clinical research and their mechanisms of antitumor action have been clearly described.[15,16] Moreover, ruthenium can display variable oxidation states (II, III and IV) under different physiologically relevant conditions. This allows the rearrangement of ligands in various ways, which has wide applications in the biological field. In addition, ruthenium complexes are stable, highly water soluble, and exhibit relatively slow ligand exchange rates in water. Furthermore, they are active against some cisplatin-resistant cell lines with low side effects due to their higher selectivity to cancer cells compared with normal cells, and thereby selectively taken up by tumours compared to healthy tissue, which is another important aspect when considering biological applications.[4,17] Ruthenium can also mimic iron in binding to certain biological molecules such as albumin and transferrin in the blood stream, which is beneficial for its delivery to cells with minimal side effects, making ruthenium complexes a suitable choice as efficient anticancer drugs.[4,17b,18,19] Accordingly, various anti-neoplastic ruthenium scaffolds have entered clinical trials, including Ru(III) species, imidazolium(imidazole)-(dimethylsulfoxide)tetrachlororuthenate(III) (NAMI-A),[19–21] indazolium *trans*-[tetrachlorobis(1*H*-indazole)ruthenate-(III)] (KP1019)[22,23] and KP1339[24] and Ru(II)-based therapeutic TLD1433.[25] However, the low therapeutic index of NAMI-A and poor solubility of KP1019 prevent their entry in phase II clinical trials.[26,27] In addition to KP1339, some other examples of clinically approved ruthenium(II)–arene complexes include AH54 and AH63, which are employed in the radio sensitization of human colorectal cancer cells and RAPTA-C in human ovarian carcinoma cells (A2780).[28] Additionally, the bioactivity of the ligands attached to the central metal ion in coordination complexes is also an important factor in drug synthesis.[29] The presence of a reducing agent, such as glutathione (GSH) and ascorbic acid in pancreas,[17c,30] results in the reduction of Ru^{III} to Ru^{II} and increases the rate of aquation and binding with biomolecules, and thus Ru in the +2 oxidation state is the active form of the drug.[31] However, a high concentration of

Department of Chemistry, School of advanced sciences, Vellore Institute of Technology, Vellore-632014, Tamilnadu, India. E-mail: priyankar.paira@vit.ac.in

†Electronic supplementary information (ESI) available. See DOI: 10.1039/D0DT02069A

glutathione can reduce the efficiency of Ru(II) complexes by binding to the metal center,[32] which leads to failure in chemotherapy.[32b,33] In addition, many anticancer agents show a decrease in activity in hypoxia.[34] Therefore, we focused our attention on designing a Ru(II)–arene complex that is (i) cytoselective, (ii) GSH resistant, (iii) hypoxia efficient and (iv) a cellular imaging agent. It is well-known that the activity of Ru(II)–arene complexes can be tuned by changing the their arene group[35] or auxiliary ligands with good leaving halide groups.[36]

Arylimidazophenanthroline compounds have been proven to be quite good for binding with metals as ligands.[37] These compounds are widely used for *in vitro* DNA synthesis, as probes of DNA structure, and new therapeutic agents due to their capacity to bind and interact with DNA. Thus, they are good cytotoxic agents in the HeLa cell line.[38–40] Gök *et al.* in 2013 and Grgurić-Šipka *et al.* in 2016 devised a series of half-sandwich η^6-arene-ruthenium(II) complexes with imidazophenanthroline moieties serving as ligands and investigated their anticancer and antibacterial activities.[41,42] In 2013, Wu *et al.* demonstrated the high anti-proliferative effect of η^6-arene-ruthenium(II) complexes with the imidazophenanthroline moiety as a ligand.[43,44] These complexes exhibited powerful inhibitory effect on various cancer cell lines with a remarkable potency towards human osteosarcoma (MG-63) cells. The intercalative binding mode of the arylimidazophenanthroline moiety helps in unwinding the double stranded DNA, thereby allowing the drug to insert into DNA and exert its function. They also predicted that the mode of action of these complexes is DNA damage-mediated p53 phosphorylation *via* S-phase cell cycle arrest. In 2012, Gan *et al.* synthesized an imidazophenanthroline moiety attached to a ruthenium complex with the formula $[Ru(bpy)_2(mbpibH_2)]^{2+}$, where bpy represents 2,2′-bipyridine and $mbpibH_2$ is 1,3-bis([1,10]phenanthroline[5,6-*d*]imidazol-2-yl)benzene, having a free coordination site, which could bind *via* intercalation or groove binding.[45] In our previous work, we achieved some breakthroughs in Ru(II)–arene-based N^N complexes for diagnosis and cancer therapy.[46] Encouraged by the excellent photophysical properties, DNA binding abilities and steric bulkiness of the π-rich arylimidazophenanthroline ligands together with their various other advantages such as enhancement of lipophilicity, triggering cellular accumulation, and good aqueous solubility of Ru(II)–arene complexes enticed us to design a few Ru(II)-*p*-cymene N^N complexes (N^N = 2-aryl-imidazophenanthroline). The complexes were synthesized *via* ultra-sonication, characterized spectroscopically and evaluated for their biological activities.

Results and discussion

Synthesis and characterization

A series of imidazo[4,5-*f*][1,10]phenanthroline ligands (**L1–L4**) was prepared by treating an equimolar mixture of 1,10-phenanthroline-5,6-dione and different aromatic carboxaldehydes (**1–4**) in the presence of ammonium acetate and glacial acetic acid, as shown in Scheme 1. The products (**L1–L4**) were fully

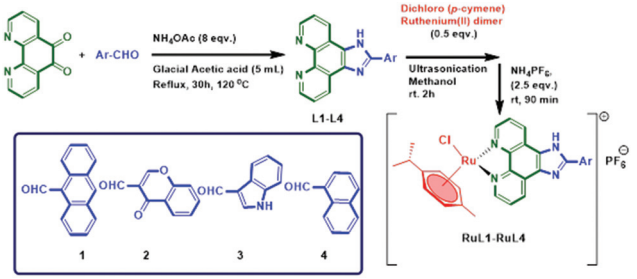

Scheme 1 Synthesis of (η^6-*p*-cymene)ruthenium(II)-imidazophenanthroline complexes.

characterised *via* nuclear magnetic resonance (NMR), Fourier transform infrared (FT-IR) and electrospray ionization mass spectrometry (ESI-MS). The structure of compound **L4** was elucidated *via* ^{1}H NMR spectroscopy as follows. All the aromatic protons of the ligand appeared in the range of 7.63–9.15 ppm. The most deshielded proton present in the naphthalene ring exhibited as doublet at δ 9.15 ppm. The other two deshielded protons, which are in close proximity to the N-atom in the phenanthroline ring, showed a doublet integrated at δ 9.06 ppm. The characteristic peak at 1391 cm^{-1} in the IR spectra can be attributed to the formation of a C–N bond. The ESI-MS peak at *m*/*z*: 347.3 $[M + H]^+$ confirms the formation of the product since it matches exactly with the theoretical value. Further to prepare Ru(II)-*p*-cymene-imidazophenanthroline complexes (**RuL1–RuL4**), $[RuCl(\mu\text{-}Cl)(\eta^6\text{-}p\text{-cymene})]_2$ was added to the prepared ligands (**L1–L4**) in a 1 : 2 ratio in methanol under ultrasonication for 2 h. After a change in colour from dark yellow to reddish brown, 2.5 equivalents of NH_4PF_6 was added and sonicated for 90 min (Scheme 1). The complexes [(η^6-*p*-cymene)-Ru^{II}(L1)Cl]PF_6 (**RuL1**), [(η^6-*p*-cymene)-Ru^{II}(L2)Cl]PF_6 (**RuL2**), [(η^6-*p*-cymene)-Ru^{II}(L3)Cl]PF_6 (**RuL3**), and [(η^6-*p*-cymene)-Ru^{II}(L4)Cl]PF_6 (**RuL4**) were obtained in good yield (92–95%) (Scheme 1).

The structures of all the complexes (**RuL1–RuL4**) were analysed *via* ^{1}H, ^{13}C, ^{19}F and ^{31}P NMR, FT-IR and ESI-MS spectroscopy. The complex **RuL4** displayed a characteristic doublet peak at 0.92 ppm, corresponding to the two methyl groups of *para* cymene and one singlet methyl peak at 2.22 ppm. The aromatic protons of *para* cymene exhibited two distinct doublet peaks in the range of 6.13–6.37 ppm. The protons of ligand **L4** experienced a considerable downfield effect upon attachment to the ruthenium *para* cymene precursor. In the ^{13}C NMR spectrum, the ligand carbons appeared at around δ 107.0–154.3 ppm. However, the new signals in the aromatic region (δ 84.2–103.9 ppm), confirmed the presence of the *p*-cymene group in complex **RuL4**. Similarly, the aliphatic CH_3 and CH carbons peaks were observed in the range of δ 18.3–30.9 ppm. In the ^{19}F NMR spectrum, characteristic peaks of six fluorines appeared at δ −69.2 and −71.08 ppm. The characteristic septate of phosphorous was observed in the range of δ −135.41 to −157.37 ppm in the ^{31}P NMR spectrum. In the FT-IR spectra, the characteristic peaks of the sp^3 C–H

stretching were observed at 3051 cm^{-1}, sp^3 C–H bending at 1408 cm^{-1} and PF stretching at 835 cm^{-1}, which indicate the formation of the Ru(II) complex. The ESI-MS peak at *m*/*z*: 619.4 $[M]^+$ and isotopic pattern of ruthenium confirmed the formation of complex **RuL4**. Similarly, a clear difference in peak values in the NMR, FT-IR and ESI-MS spectra between the other ligands (**L1–L3**) and their corresponding complexes (**RuL1–RuL3**) were observed (ESI†).

Photophysical study

The absorption and emission spectra of all the complexes (**RuL1–RuL4**) at 298 K were recorded in a DMSO–water (1 : 1) solvent system, as shown in Fig. S1.† The photophysical data is summarized in Table 1. The characteristic intraligand (π–π^*) transitions (N^N ligands) appeared at 250–350 nm and metal-to-ligand charge transfer (^{1}MLCT) at 360–480 nm.[47,48] Among the complexes, we observed the maximum absorption in the ^{1}MLCT region for the anthracene derivative (**RuL1**). The MLCT peak underwent a blue shift together with an increase in ε value for **RuL1**. In the emission spectra, we observed the MLCT emission of all the complexes in the range of 400–600 nm (Fig. S1†). Similar to the absorption spectra, the emission for the anthracene derivative is the most intense because of its strong π conjugation. Using the emission spectral data, the quantum yield of the complexes was calculated using eqn (ii). Among the four complexes, complex **RuL1** showed the highest quantum yield (0.128) for the MLCT transition (Table 1).

Solubility, lipophilicity and conductivity

Both hydrophilicity and lipophilicity studies were performed to determine the tumour-inhibiting potential of the metal complexes. These complexes were highly soluble in DMSO and moderately soluble in H_2O, MeOH, EtOH and CH_3CN. Furthermore, they were soluble in the range of 5–10 mg per mL of DMSO–10% DMEM medium (1% DMSO in DMEM, 1 : 99 v/v, comparable to cell media) at 25 °C (Table 1). The lipophilicity of these complexes was determined by performing an *n*-octanol/water partition coefficient ($\log P_{o/w}$, where $P_{o/w}$ = the octanol/water partition coefficient) study using the shake flask method (Table 1).[49] The experimental $\log P_{o/w}$ values of these complexes were determined to be in the range of 0.42–1.01 (Table 1). Complex **RuL1** exhibited the highest $\log P_{o/w}$ due to the hydrophobic nature of its anthracene group. The lowest $\log P_{o/w}$ value was observed for compound **RuL3** because its hydrophilic indole –NH group. The ruthenium complexes **RuL1–RuL4** exhibited molar conductance values in the range of ~20–23 S m^2 M^{-1} in pure DMSO. Furthermore, their molar conductance increased in 10% DMSO (~109–128 S m^2 M^{-1}, Table 1), suggesting their 1 : 1 and 1 : 2 electrolytic nature in pure DMSO and 10% DMSO, respectively.[50]

This change in the electrolytic behaviour of the complexes from 1 : 1 to 1 : 2 can be attributed to the dissociation of the Ru–Cl bond and subsequent aquation of the complexes. The ionic strength (*I*) of these complexes was calculated to be $I = 9 \times 10^{-5}$ M ($I = \frac{1}{2} \times Æ©CiZi^2$). Furthermore, the gradual increase in the conductivity of the complexes with incubation time in 10% DMSO suggests the ease of departure of the labile –Cl group from the complexes, easily justifying the 1 : 2 electrolytic nature of the complexes. Together with this, the increase in conductivity with an increase in the concentration of CT-DNA and GSH also depicts the aquation of the complexes due to the breaking of the Ru–Cl bond. Additionally, the increase in conductivity at the low pH of cancer cells confirmed the aqua complex formation exposing the 1 : 2 electrolytic nature of the complexes (Fig. S2–S5†). Thus, all these results afford satisfactorily support for the DNA covalent interaction *via* aqua complex formation in the cancer environment (low pH and high GSH).

Stability study

The stability studies of two complexes, *e.g.* **RuL1** and **RuL4**, were conducted in two different solvents, *i.e.* aqueous DMSO (H_2O : DMSO = 9 : 1) and aqueous GSH medium (Fig. S6 and S7†), respectively. It is essential that the complexes remain stable in the biological environments of cells, and thus the stability studies were performed. The obvious change in absorbance (~15–30% decrease after 24 h) for both complexes with time in aqueous DMSO clearly revealed the moderate dissociation of the –Cl ligand from the Ru(II) complexes followed by aqua complex formation, which was also quantitatively determined based on the observed molar conductivity of the complexes (**RuL1–RuL4**) in aqueous DMSO. However, the steric bulkiness of the arylimidazophenanthroline ligand may slow down the hydrolysis of the Ru(II) complex.[51] Glutathione is a key detoxifying agent in the presence of glutathione

Table 1 Photophysical characterization, solubility, lipophilicity and conductivity study of the complexes (**RuL1–RuL4**)

								$\Lambda_M{}^g$ (μs)	
Sample	$\lambda_{max}{}^a$ (nm)	$\lambda_f{}^b$ (nm)	Stokes shift	$\varepsilon{}^c$ (M^{-1} cm^{-1})	$(\varphi_f)^d$	Solubility^e (M)	Log P^f	DMSO	10% DMSO
RuL1	390	425, 450	35, 60	13 333	0.128	0.024	1.01 ± 0.12	21	109
RuL2	390	420	30	6666	0.119	0.021	0.72 ± 0.08	20	112
RuL3	390	440	50	10 000	0.027	0.014	0.42 ± 0.08	21	110
RuL4	390	440	50	3333	0.029	0.019	0.99 ± 0.20	23	128
Quinine sulphate	350	452	102	—	0.546	—	—	—	

[a] Absorption maxima. [b] Maximum emission wavelength. [c] Extinction coefficient. [d] Quantum yield. [e] DMSO–10% DMEM medium (1 : 99 v/v, comparable to cell media). [f] *n*-Octanol/water partition coefficients. [g] Conductance in DMSO and 10% aqueous DMSO (**RuL1–RuL4**; 3×10^{-5} M).

S-transferase (GST) in cells.[52] It has been reported that many cancer cells become resistant to various drugs by increasing their cellular glutathione level.[53] Hence, to determine the effect of GSH on the reported complexes, a stability study was performed in the presence of excess (10 eq.) glutathione (GSH) *via* time-dependent UV spectroscopy. However, we observed the similar results to that in aqueous DMSO.

These results revealed the following two mechanisms: (i) the aqua complex facilitates the transportation of these compounds into the cytoplasm through serum albumin and they bind with DNA *via* covalent bonding and (ii) deactivation of these complexes is expedited through the GSH–drug covalent interaction. Therefore the tendency for aqua complex formation due to the dissociation of the Ru–Cl bond promotes the drug to be GSH resistant in the cancer cell environment.

DNA binding study

UV absorption method. To design effective chemotherapeutic drugs, it is essential to explore the interactions of metal complexes with DNA. The most commonly used methods to determine the type of interaction involved between metal complexes and DNA is electronic absorption titration. There are three different modes of non-covalent interaction between small molecules and DNA: (i) intercalation, (ii) partially intercalation, and (iii) groove binding, which can be stabilized by hydrogen, electrostatic, and hydrophobic bonding interactions. These interactions display the mechanism of action and effectiveness of metallodrugs. Both complexes displayed two strong absorption bands at 250 nm and 300 nm, corresponding to the intraligand π–π* transition. The weak absorption peaks of the Ru(dπ)–imidazophen(dπ*) charge transfer (MLCT) transitions were observed in the range of 360–480 nm (Fig. S8†). DNA base pairs such as purine (adenine and guanine) and pyrimidine (cytosine and thymine) analogues are responsible for electronic transitions. Upon the addition of CT-DNA in increasing concentration from 5 μM to 60 μM, we observed a hypochromic shift in both π–π* and the MLCT region in case of complex **RuL1**. In contrast, for **RuL4**, there was a hyperchromic shift in absorbance at 250 nm and hypochromic shift in absorbance at 300 nm, resulting in the appearance of an isosbestic point, which indicates the prevalence of covalent interaction of the complex with DNA together with the intercalative mode of interaction.

However, there was no significant change in the absorbance of complex **RuL4** in the MLCT region with the gradual addition of DNA. Also, there was a slight increase in wavelength (bathochromism) for both complexes during the course of the study. The extent of hypochromism and bathochromism commonly specify the intercalative binding strength.[54,55] Significant hyperchromism may be attributed to external contact (electrostatic binding), covalent binding, groove binding or partial uncoiling of the helix structure of DNA, exposing more bases of DNA.[54,55] The planarity of the anthracene moiety in the **RuL1** complex can result in the remarkable intercalative mode of interaction with DNA, as suggested by the hypochromism in the absorbance intensity during the DNA binding study. Simultaneously, the slight obstruction in the release of the –Cl group from the complex due to the steric bulkiness of anthracene moiety can subdue the covalent binding mode of the drug with DNA.[51] Therefore, in the case of **RuL1**, hypochromism alone was observed. On the other hand, the appearance of an isosbestic point as a result of both hypo- and hyperchromism in the absorbance spectrum of complex **RuL4** provides information about the prevalence of the covalent binding mode together with intercalation since the planarity and steric bulkiness are diminished in the case of naphthalene moiety compared to the anthracene moiety. The intrinsic binding constant (K_b) for both complexes (**RuL1** and **RuL4**) were determined using eqn (i) (see ESI†) and from the [DNA]/($\varepsilon_a - \varepsilon_f$) *vs.* [DNA] linear plots (Table 2 and Fig. S9†). Compound **RuL1** exhibited a significant (10^5) $K_{b\pi-\pi^*}$(2.0×10^5 M^{-1}, λ_{max} = 250 nm), $K_{b\pi-\pi^*}$ (0.6×10^5 M^{-1}, λ_{max} = 300 nm) and K_{bMLCT} (0.35×10^5 M^{-1}, λ_{max} = 380 nm) values, which were slightly lower than that of the classical DNA intercalator ethidium bromide (EthB) ($K_{EthB} = 7 \times 10^5$ M^{-1}).[56] Furthermore, complex **RuL4** also displayed a similar order of intrinsic binding constant $K_{b\pi-\pi^*} = 0.75 \times 10^5$ M^{-1} at λ_{max} = 300 nm only (Table 2).

EtBr quenching study

The competitive binding of compounds **RuL1** and **RuL4** to CT-DNA was studied *via* fluorescence spectroscopy using ethidium bromide (EtBr) as the fluorophore. We clearly observed a gradual decrease in the fluorescence intensity of the EtBr-bound DNA in the presence of the complexes since they displaced EtBr from DNA, and consequently got bound between the base pairs of the DNA, suggesting the intercalative binding mode of action, as observed in Fig. S10.†

Table 2 DNA binding parameters for complexes **RuL1** and **RuL4** with CT-DNA

Complex	λ_{max} [nm]	Change in absorbance	$\Delta\varepsilon^a$ (%)	$K_b{}^b$ ($\times 10^5$ M^{-1})	$K_{sv}{}^c$ ($\times 10^6$ M^{-1})	$K_{app}{}^d$ ($\times 10^6$ M^{-1})
RuL1	250	Hypochromism	60	2.00	0.01	2.67
	300	Hypochromism	62	0.60		
	380	Hypochromism	66	0.35		
RuL4	250	Hyperchromism	35	—	0.03	2.67
	300	Hypochromsim	50	0.75		

[a] % Change in hypochromism or hyperchromism. [b] K_b, intrinsic DNA binding constant from UV–visible absorption titration. [c] K_{sv}, Stern–Volmer quenching constant. [d] K_{app}, apparent DNA binding constant from competitive displacement.

The compound was excited in presence of EtBr-bound DNA at 485 nm and its fluorescence emission was recorded at 598 nm. The concentrations of the other reagents involved are as follows: [DNA] = 120 μM, [EtBr] = 8 μM, $[\mathbf{RuL1}]_{50}$ = 30 μM, and $[\mathbf{RuL4}]_{50}$ = 30 μM. The calculated K_{app} according to eqn (iii) for both complexes **RuL1** and **RuL4** was observed to be $K_{app} = 2.67 \times 10^6\ M^{-1}$. The Stern–Volmer quenching constant, K_{SV}, was calculated in accordance with eqn (iv), and was found to be $0.01 \times 10^6\ M^{-1}$ for complex **RuL1** and $0.03 \times 10^6\ M^{-1}$ for complex **RuL4** (Fig. S11†). The significant change in the spectral band position (hypochromism and hyperchromism, $\Delta\varepsilon$ = 50–66%), high intrinsic binding constant ($K_b \sim 10^5$) and high apparent binding constant ($K_{app} \sim 10^6$) suggested the strong binding of these complexes with DNA. The mode of DNA interaction of these complexes was further confirmed by viscosity measurement. In addition, the high value of hypochromism ($\Delta\varepsilon$ = 50–66%), high K_b (~0.35–2.0 × $10^5\ M^{-1}$) and high K_{app} ($2.67 \times 10^6\ M^{-1}$) of both complexes suggest intercalation with CT-DNA.[47] The observed K_b values of **RuL1** and **RuL4** were higher than that reported for Ru(II)–arene complexes[57] and lower than that of Ru–polypyridyl complexes such as $[Ru(pdto)(dppz)]^{2+}$ (K_b, $3.0 \times 10^6\ M^{-1}$),[58] $[Ru(phen)_2(dppz)]^{2+}$ (K_b, $5.1 \times 10^6\ M^{-1}$)[58] and $[Ru(bpy)_2(dppz)]^{2+}$ (K_b, $1.3 \times 10^6\ M^{-1}$).[58b]

Viscosity method

To determine the binding mode of drugs with DNA, a hydrodynamic method such as a viscosity experiment is usually conducted. The viscosity study of complex **RuL4** demonstrated its intercalative nature with an increase in its concentration and its covalent binding ability to DNA with a decrease in its concentration. This complex exhibited significant intercalation in the range of 50 μM to 80 μM, which was clear from the steepness of the line in the viscosity graph (Fig. S12†). Subsequently, the slow increase in the steepness of line from 80 μM and higher indicates its moderate intercalative power with DNA base pairs. On the other hand, with a decrease in concentration of the complex from a higher concentration as a function of DNA concentration, a steady decrease in viscosity was observed. This suggests that DNA will induce the complex molecule to bind in a covalent manner by replacing its labile chlorine coordinated to the metal in the complex moiety. These results were also compared with the viscosity plot of EtBr with DNA (Fig. S12†). Hence, both types of interactions may prevail to destroy the nucleus of cancerous cells depending on the concentration of the drug.

BSA binding study

Upon excitation at 295 nm, the emission intensity of BSA at λ_{em} = 350 nm decreased gradually on increasing the complex concentration, which confirmed that the interaction between complexes **RuL1** and **RuL4** with BSA had occurred, as observed in Fig. S13.† The Stern–Volmer quenching constant of these complexes with BSA (K_{BSA}) was calculated using the Stern–Volmer eqn (v) and the corresponding Stern–Volmer plots (Fig. S14†). The binding affinity (K) of the complexes was calculated from Scatchard plot analysis and using eqn (vi) (Fig. S15†). The complexes showed strong binding propensity with BSA, which is required for the transport of protein-bound complexes in biological systems. As depicted in Table 3, the K_{BSA} for complex **RuL1** was found to be $0.38 \times 10^6\ M^{-1}$ and that for complex **RuL4** was $0.01 \times 10^6\ M^{-1}$, whereas, the K value for **RuL1** was $1.25 \times 10^4\ M^{-1}$ and $1.51 \times 10^4\ M^{-1}$ for **RuL4**. The value of bimolecular quenching constant (k_q) calculated from K_{SV} and τ_0 (1×10^{-8} s) was observed to be $3.8 \times 10^{13}\ M^{-1}\ S^{-1}$ for complex **RuL1** and 0.99×10^{12} for complex **RuL4**. These values are higher than the maximum possible value for dynamic quenching ($2.0 \times 10^{10}\ L\ mol^{-1}\ s^{-1}$),[59,60] suggesting the involvement of static quenching mechanism by the present Ru(II) arene complexes. It is well known that in many cases, fluorophores can be quenched by both collision (dynamic quenching) and complex formation with the same quencher (static quenching).[59,60] Herein, the high value of the quenching rate constant, k_q (10^{12}–$10^{13}\ M^{-1}\ S^{-1}$), indicates effective bimolecular quenching together with binding.[59,60] The Stern–Volmer plot shown in Fig. S14b† exhibits an upward curvature, concave toward the *Y*-axis at a high quencher concentration. This nonlinear Stern–Volmer plot of complex **RuL1** indicates that both static and dynamic quenching processes contributed to the overall quenching of BSA. The non-linearity of the Stern–Volmer plot of **RuL1** is due to the formation of a ground state complex between the Ru(II) complex and BSA.

Table 3 Binding parameters of complexes **RuL1** and **RuL4** with BSA

Complex	K_{BSA} [a] $[M^{-1}]$	k_q [b] $[M^{-1}s^{-1}]$	K [c] $[M^{-1}]$	n [d]
RuL1	0.38×10^6	3.8×10^{13}	1.25×10^4	1.7
RuL4	0.01×10^6	0.99×10^{12}	1.51×10^4	0.7

[a] K_{BSA}, Stern Volmer quenching constant. [b] K_q, quenching rate constant. [c] K, binding constant with BSA. [d] n, number of binding sites.

In vitro cytotoxicity study

The *in vitro* cytotoxicity of complexes **RuL1–RuL4** and cisplatin were investigated using the typical 3-(4,5-dimethylthiazol-2-yl)-2,5-diphenyltetrazolium bromide (MTT) assay protocol and a panel of cancer cell lines, *i.e.* human epithelioid cervix carcinoma (HeLa), colorectal adenocarcinoma cells (Caco-2), and one normal cell line, *i.e.* human embryonic kidney cells (HEK-293), in triplicate. Complex **RuL4**, with IC_{50} values ranging from 2–4 μM, showed much higher cytotoxicity than complexes **RuL1**, **RuL2**, and **RuL3** and both positive controls (cisplatin and RAPTA-C) against all the human cancer cell lines tested (Table 4). Interestingly, the synthesized complexes exhibited much higher potency than RAPTA-C in both cancer cell lines. In terms of selectivity, all the compounds were 2–40-fold more selective for cancer cells than the positive controls. Notably, complex **RuL4** exhibited 24- and 40-fold higher selectivity against HeLa and Caco-2 cells over non-cancerous HEK-293 cells, respectively. A compound having a good *in vitro* cytotoxicity profile under normoxia may be a good sign, but its cytotoxicity may deteriorate under hypoxic environments due

Table 4 MTT cytotoxicity screening of Ru(II)–arene complexes (**RuL1–RuL4**) and control

	IC_{50} (μM) ± S.D.[a]											
	Normoxia			SF[b]		Normoxia + GSH[e]		Hypoxia[f]		Hypoxia + GSH	
Complex	HeLa[c]	CaCo-2[d]	HEK-293	HeLa	CaCo-2	HeLa	CaCo-2	HeLa	CaCo-2	HeLa	CaCo-2
RuL1	22.9 ± 1.3	SF[b]	>100	>4.6	>4.9	27.0 ± 1.4	23.7 ± 1.2	23.0 ± 1.6	21.4 ± 1.2	28.1 ± 1.2	23.6 ± 1.5
RuL1	27.5 ± 1.9	14.2 ± 1.4	>100	>3.6	>7.0	29.4 ± 1.1	17.8 ± 1.1	28.8 ± 1.2	14.6 ± 1.4	30.0 ± 1.4	18.7 ± 1.2
RuL3	47.1 ± 1.4	34.5 ± 2.7	>100	>2.1	>2.6	51.0 ± 1.3	38.9 ± 1.8	47.8 ± 1.4	38.0 ± 1.2	48.2 ± 1.6	40.8 ± 1.5
RuL4	4.1 ± 1.2	2.5 ± 0.9	>100	>24.4	>40.0	5.9 ± 1.0	2.6 ± 1.2	5.2 ± 1.1	2.8 ± 0.7	5.3 ± 1.0	2.7 ± 1.1
Cisplatin	21.8 ± 0.8	14.2 ± 1.4	24.4 ± 1.5	1.1	1.7	34.7 ± 1.2	21.5 ± 0.8	29.3 ± 1.4	35.4 ± 1.4	42.6 ± 1.8	36.3 ± 1.5
RAPTA-C	246.9 ± 1.2	>300	>300	>1.2	1	ND[g]	ND	ND	ND	ND	ND

[a] IC_{50} is the concentration at which 50% of cells undergo cytotoxic cell death due to organoruthenium, cisplatin and RAPTA-C treatment in triplicate. It was calculated by non-linear sigmoidal curve fitting of the dose–response model using Origin 8.5. Each value represents the mean ± SD (standard deviation) of three independent experiments. [b] SF (selectivity factor) = ratio of IC_{50} for HEK-293 and IC_{50} for all the cancer cell lines. HEK-293 fibroblasts are generally selected as the model for healthy cells in the evaluation of chemotherapeutic drug selectivity. [c] 48 h incubation time for HeLa. [d] 72 h incubation time Caco-2 cell line. [e] GSH = reduced glutathione (1 mM). [f] Hypoxia (1% O_2). Statistical significance is indicated as $P < 0.05$ based on the Student's *t*-test using the Origin 8.5 software (the statistical significance (p) of the data is <0.05 or better). [g] ND = not determined.

to hypoxia-induced resistance.[34] Hence, we explored the activity of these complexes under hypoxic (O_2, 1%) conditions in HeLa and CaCo-2 cells. We found an insignificant change in the IC_{50} values of these complexes under hypoxia compared to normoxia, suggesting their efficiency in extreme hypoxic cellular conditions (Table 4 and Fig. 1). For example, complex **RuL4** showed IC_{50} values of 4.1 ± 1.2 μM ($p < 0.05$) and 2.5 ± 0.9 μM ($p < 0.001$) under normoxia against HeLa and CaCo-2 cells, respectively (Table 4 and Fig. 1). Similarly, we found that the IC_{50} values of this complex were 5.2 ± 1.1 μM ($p < 0.05$) and 2.8 ± 0.7 μM ($p < 0.0001$) against hypoxic HeLa and CaCo-2 cells, respectively (Table 4 and Fig. 1). In contrast, cisplatin displayed a massive decrease in activity (~50%) under identical hypoxic conditions (Table 4 and Fig. 1).[34b] These results suggest that complex **RuL4** are equally potent under normoxia and hypoxia with high selectivity, which is a significant quality for an anticancer agent.[34a] Since the synthesized complexes **RuL1** and **RuL4** showed moderate interaction with L-glutathione in the UV-Vis study, these compounds are expected to be deactivated by GSH.[33d,e] To confirm this suspicion, we probed the activity of all the synthesized complexes under normoxic conditions in the presence of 1 mM of reduced L-glutathione against HeLa and CaCo-2 cells. All the complexes displayed a slight loss in activity under the normoxic condition in the presence of externally added GSH in the culture media; however, the deactivation was very low.

This may be described in two ways as follows: (i) the Ru(II) complexes exhibited a higher order of affinity (~10^{12}–10^{13}) to serum albumin, which protected them from deactivation by GSH and assisted their delivery to the target site[51,61,62] and (ii) the GSH reacted competitively with oxygen; hence, the deactivation of the Ru(II) complexes was low. It is well known that cancer cells in hypoxic regions are usually resistant to both radiotherapy and chemotherapy.[63] Thus, to determine the exact reason behind the significant potency of these complexes in the presence of a high GSH concentration we evaluated their *in vitro* toxicity towards hypoxic (O_2, 1%) cancer cells in the presence of excess reduced glutathione (Table 4 and Fig. 1).[64] However, there were no significant differences in activity observed for all the complexes under the normoxia and hypoxia condition. These results reveal the significance of serum albumin rather than a normoxic cellular O_2 level for combating GSH, stopping the deactivation process. All four complexes exhibited much higher cytotoxicity in normoxic, normoxic GSH, hypoxic and hypoxic GSH media towards the cancer cell lines compared to cisplatin.

Cellular uptake and imaging study

We quantified the cellular uptake levels of the Ru(II) complexes (**RuL1–RuL4**) using inductively coupled plasma mass spectrometry (ICP-MS). After incubation with the Ru(II) complexes (5 μM) for 24 h, as can be seen in Fig. 2, the ICP-MS results revealed that high levels of complexes **RuL1–RuL4** were accumulated in the HeLa cells. The cellular Ru accumulation was observed to follow the trend of **RuL4** > **RuL1** > **RuL2** > **RuL3** (Fig. 2). However, the difference in Ru accumulation between **RuL1** and **RuL2** was very small. The cellular accumulation data was correlated with the lipophilic nature ($\log P_{o/w}$ values) of the complexes. Due to the hydrophilic –NH in indole, complex **RuL3** was less accumulated inside the cells. The trend of this accumulation was also in agreement with the cytotoxicity profiles (Table 4 and Fig. 1). RAPTA-C exhibited much lower accumulation in the HeLa cells compared to all the synthesized Ru(II)-*p*-cymene complexes (**RuL1–RuL4**).

We performed the cellular imaging experiment using the HeLa cell line. HeLa cells were incubated with fresh Dulbecco's modified Eagle's medium (DMEM, with 1% pen/strep and 10% FBS) containing 20 μM of the most fluorescent complex **RuL1** (in DMSO/culture medium, 1/99, v/v) for 4 h at 37 °C, and then washed them gently with PBS. The images were taken using an Olympus fluorescence microscope under 480 nm excitation. Live cells were traced by the red fluorescence of compound **RuL1** under the fluorescence microscope (Fig. 3). This result clearly indicated the strong cellular

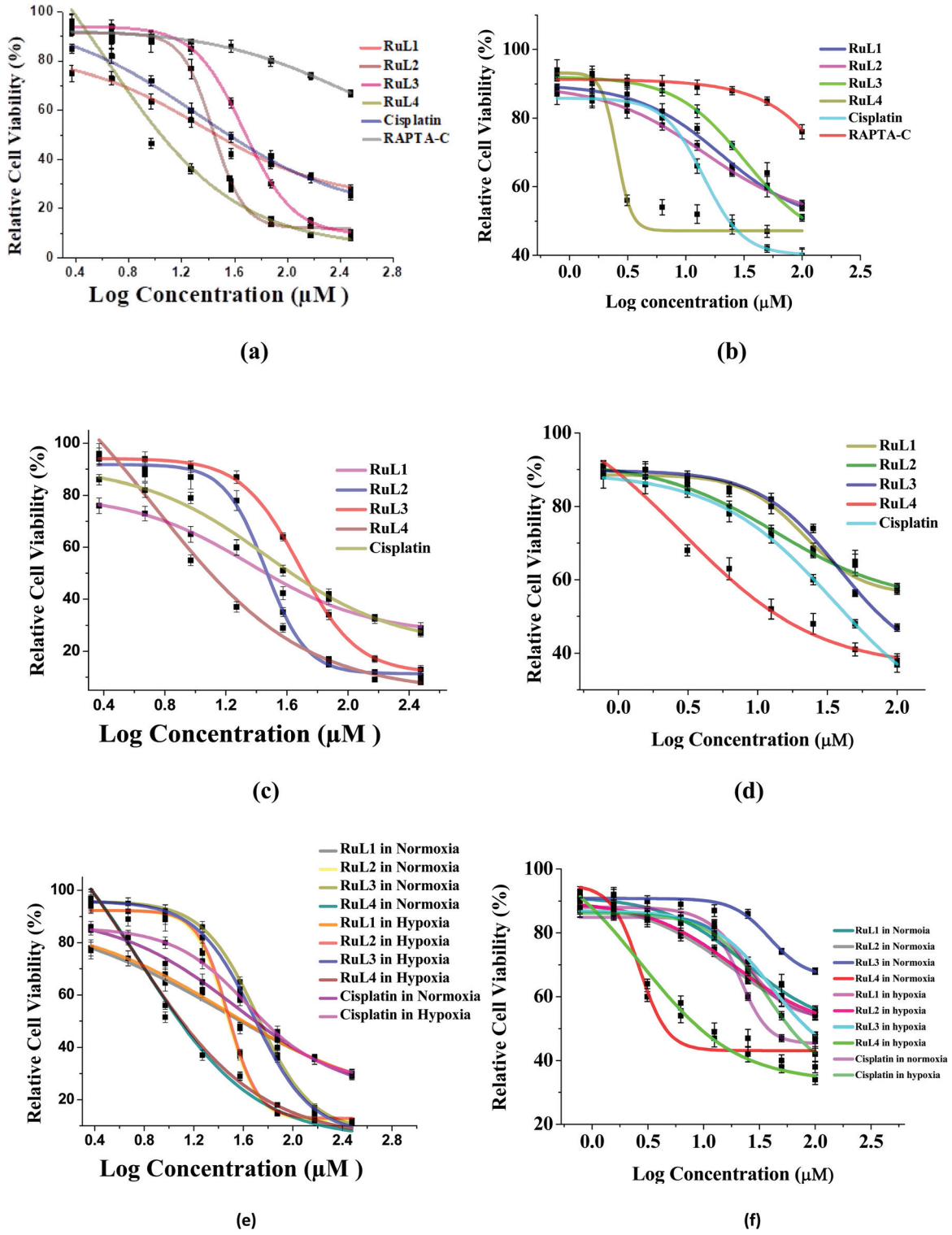

Fig. 1 Comparison of the cytotoxicity of complexes **RuL1–RuL4**, cisplatin and RAPTA-C in (a) normoxic condition against HeLa cells, (b) normoxic condition against CaCo-2 cells, (c) hypoxic condition against HeLa cells, (d) hypoxic condition against CaCo-2 cells, (e) both conditions in the presence of GSH against HeLa cells and (f) both conditions in the presence of GSH against CaCo-2 cells. Cytotoxicity of RAPTA-C was not evaluated in hypoxia and GSH media.

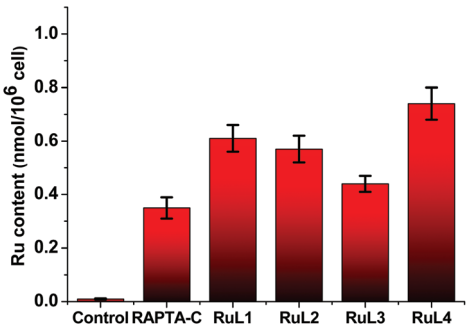

Fig. 2 Ruthenium content inside HeLa cells treated with complex **RuL1–RuL4** and RAPTA (5 μM) for 24 h. Data obtained from ICP-MS analysis. Error bar shows the standard error of the data.

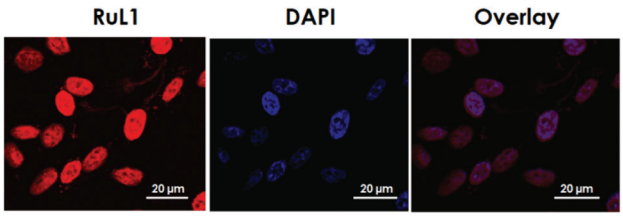

Fig. 3 Co-localization images of **RuL1** complex (20 μM) in live HeLa cells after 4 h of incubation with nucleus dye DAPI. Excitation wavelength was 480 nm. Scale bar 20 μm.

uptake of complex **RuL1** upon 4 h incubation with the HeLa cell line. Co-localization of the complex with DAPI showed that the intracellular distribution of this complex is mainly in the nucleus compared to the other organelles (Fig. 3).

Experimental

Materials and methods

In all the experiments, the reagents and solvents used were of the highest grade and best commercial quality. All organic solvents used throughout the chemical synthesis and chromatography procedures were of analytical grade and used without further purification as-received from E. Merck (India). Dichloro-*p*-cymene ruthenium(II) chloride dimer, 1,10-phenanthroline-5,6-dione, α-naphthaldehyde, 9-anthraldehyde, chromone-3-carboxaldehyde, and indole-3-carboxaldehyde were procured from Sigma Aldrich Chemical Ltd, Merck and Spectrochem. Thin layer chromatography was performed on pre-coated silica gel 60 F_{254} aluminium sheets (E. Merck, Germany) and the solvent system was an ethyl–acetate–methanol mixture. Bovine serum albumin (BSA) was purchased from Sigma Aldrich Chemical Limited. The HeLa and HEK-293 cell lines were purchased from NCCS, Pune. The caco-2 cell line was procured from ATCC, Sigma Aldrich. ^{1}H NMR, ^{13}C NMR, ^{19}F NMR and ^{31}P NMR spectra were recorded on a 400 MHz Advance Bruker DPX spectrometer with tetramethylsilane (TMS) as the internal standard. The chemical shifts were reported in ppm units. Abbreviations are as follows: s, singlet; d, doublet; dd, double doublet; t, triplet; and m, multiplet. The melting points of the complexes were measured on an Elchem Microprocessor-based DT apparatus using an open capillary tube. FT-IR spectra were recorded on a Shimadzu Affinity FT-IR spectrometer in the range of 4000–400 cm^{-1}. The mass spectra of the synthesized compounds were recorded on a Shimadzu ESI-mass spectrometer having a 4000 triple quadrupole MS, using methanol as the solvent. UV-Visible spectra were recorded on a JASCO V-730 spectrometer using a 1 cm quartz cell and fluorescence spectra on Hitachi F7000 fluorescence spectrophotometer equipped with a xenon lamp. A PerkinElmer instrument was used for the elemental analysis. The conductivity and viscosity study were performed using a conductivity-TDS meter-307 and Ostwald viscometer, respectively. For the cytotoxicity (MTT) assay and imaging study, an Elisa reader, 96-well plate, Olympus CX41 fluorescence microscope were used.

Synthetic procedures

Synthesis of arylimidazophenanthroline ligands [L1–L4]. Briefly, 50 mg (0.238 mmol, 1 equiv.) of 1,10-phenanthroline-5,6-dione and an equimolar amount of different aromatic carboxaldehydes (1 equiv.) (**1–4**) were dissolved in 5 mL of glacial acetic acid in a 50 mL round-bottom flask. Subsequently, 10 molar equivalent of ammonium acetate (183.6 mg, 2.379 mmol) was added to the reaction mixture. Then the reaction was refluxed for 30 h at 120 °C under an inert atmosphere. The completion of the reaction was monitored by TLC using 100% ethyl acetate. The contents of the reaction mixture were then transferred to a beaker and cold water was added to it. Ammonia solution was added dropwise to neutralize the highly acidic environment. The appearance of precipitate confirmed the formation of the product. The beaker was kept in the fridge overnight to allow the precipitate to settle. The contents of the beaker were then filtered, and the precipitate was dried and then subjected to repeated washing with hexane to obtain the purified product. The pure product obtained from ethyl acetate appeared to be various shades of brown and yellow with 92%–95% yield. The formation of the product was confirmed by ^{1}H NMR, ^{13}CNMR, FT-IR and ESI-MS.

*[2-(Anthracen-9-yl)-1H-imidazo[4,5-f][1,10]phenanthroline]**(L-1)**.* Yield: 92%; Mp: >300 °C; R_f (pure ethyl acetate): 0.65; IR (cm^{-1}): ν Ar C–H stretching (3046), C–N stretching (1348), C–H bending (729); ^{1}H NMR (DMSO-d_6, 400 MHz): δ 7. 04 (t, 2H, J = 7.6 Hz, ArH), 7.24 (d, 2H, J = 8.8 Hz, ArH); 7.76 (m, 2H, J = 6.4 Hz, ArH); 7.93 (d, 2H, J = 9.2 Hz, ArH), 8.13 (d, 2H, J = 8.4 Hz, ArH), 8.31 (s, 1H, ArH), 8.66 (d, 2H, J = 8.0 Hz, ArH), 8.89 (d, 2H, J = 8.4 Hz, ArH); ^{13}C NMR (DMSO-d_6, 100 MHz): δ 123.9, 124.8, 125.7, 126.0, 126.2, 126.3, 126.7, 127.2, 128.8, 129.0, 129.4, 129.8, 131.1, 131.8, 135.1, 135.8, 146.1, 148.8, 151.9, 153.5; ESI-MS (MeOH): m/z = 397.1.

*[3-(1H-Imidazo[4,5-f][1,10]phenanthrolin-2-yl)-4H-chromen-4-one]**(L-2)**.* Yield: 95%; Mp: 250–252 °C; R_f (pure ethyl acetate): 0.55; IR (cm^{-1}): ν Ar C–H stretching (3248), Ar C=C stretching (1647), C–N stretching (1462), C–H bending (758); ^{1}H NMR

(DMSO-d_6, 400 MHz): δ 7.63–7.67 (m, 1H, ArH); 7.81–7.85 (m, 4H, ArH); 7.92–7.96 (m, 2H, ArH); 8.30 (d, 1H, J = 8.0 Hz, ArH); 9.04 (d, 2H, J = 3.2 Hz, ArH), 9.33 (s, 1H, ArH); ^{13}C NMR (DMSO-d_6, 100 MHz): δ 113.8, 118.2, 120.1, 122.7, 124.7, 125.8, 126.0, 132.1, 132.7, 134.6, 135.7, 142.6, 146.0, 153.3, 155.0, 157.9, 173.8; ESI-MS (MeOH): m/z = 365.3.

*[2-(1H-Indol-3-yl)-1H-imidazo[4,5-f][1,10]phenanthroline](**L-3**).* Yield: 92%; Mp: 262–264 °C; R_f (pure ethyl acetate): 0.56; IR (cm^{-1}): ν Ar C–H stretching (3132), Ar C=C stretching (1574), C–N stretching (1358), C–H bending (735); ^{1}H NMR (DMSO-d_6, 400 MHz): δ 7.39–7.43 (m, 2H, ArH), 7.78–7.82 (m, 2H, ArH), 7.96 (d, 1H, J = 7.6 Hz, ArH); 8.04 (d, 1H, J = 7.6 Hz, ArH); 8.22 (s, 1H, ArH); 8.91 (d, 2H, J = 8.0 Hz, ArH); 9.01 (d, 1H, J = 4.0 Hz, ArH); ^{13}C NMR (DMSO-d_6, 100 MHz): δ 107.0, 112.4, 120.8, 122.0, 122.8, 123.8, 124.8, 125.6, 126.3, 130.3, 132.9, 136.2, 136.9, 138.3, 143.3, 147.8, 149.5, 156.5; ESI-MS (MeOH): m/z = 336.5.

*[2-(Naphthalene-1-yl)-1H-imidazo[4,5-f][1,10]phenanthroline](**L-4**).* Yield: 95%; Mp: 260–262 °C; R_f (pure ethyl acetate): 0.62; IR (cm^{-1}): ν Ar C–H stretching (3163), Ar C=C stretching (1537), C–N stretching (1391), C–H bending (737); ^{1}H NMR (DMSO-d_6, 400 MHz): δ 7.63–7.70 (m, 2H, ArH); 7.72–7.77 (m, 1H, ArH), 7.85 (dd, 2H, J_1 = 8.0 Hz, J_2 = 4.4 Hz, ArH); 8.09 (d, 1H, J = 8.8 Hz, ArH); 8.13–8.17 (m, 2H, ArH); 8.99 (d, 2H, J = 9.2 Hz, ArH); 9.06 (d, 2H, J = 4.4 Hz, ArH); 9.15 (d, 1H, J = 8.4 Hz, ArH); ^{13}C NMR (DMSO-d_6, 100 MHz): δ 124.1, 124.5, 125.8, 125.9, 126.6, 126.9, 127.4, 127.7, 128.5, 128.9, 129.2, 129.6, 130.2, 130.6, 130.7, 130.9, 131.3, 133.7, 134.1, 135.8, 137.4, 143.5, 148.3, 151.1; ESI-MS (MeOH): m/z = 347.3.

Synthesis of [(η^6-*p*-cymene)-Ru^{II}(arylimidazophenanthroline)Cl]PF$_6$ complexes [RuL1–RuL4]. 20 mg (0.033 mmol, 1 equiv.) of dichloro(*p*-cymene)ruthenium(II) dimer ([RuCl(μ-Cl)(η^6-*p*-cymene)]$_2$) was dissolved in about 10 mL of methanol in a 50 mL round-bottomed flask and stirred continuously for 5–10 min to dissolve the reactant. To the completely dissolve the solution, 2.1 equivalents of the previously synthesized ligands (**L1–L4**) was added and kept for 90 min under ultrasonication at room temperature. After 90 min, 2.5 equivalents of ammonium hexafluorophosphate (NH_4PF_6) (13.3 mg, 0.082 mmol) was added as the ligand exchange salt to increase the crystallinity, and hence, purity of the product, and again the reaction mixture was subjected to ultra-sonication for 90 min at room temperature. The progress of the reaction was confirmed by TLC. After complete conversion of the starting materials to the desired product, the solvent was evaporated under reduced pressure. The crude product was washed with hexane and further recrystallized from diethyl ether/methanol (1 : 1) solvent system. Finally, the complexes (**RuL1–RuL4**) were obtained as light brown crystals with a high yield (92–95%).

*[(η^6-p-Cymene)Ru^{II}Cl{K^2-N,N-(2-(anthracen-9-yl)-1H-imidazo[4,5-f][1,10]phenanthroline)}]PF$_6$ (**RuL1**).* 50.4 mg (0.062 mmol, 95%); Mr ($C_{37}H_{30}N_4ClF_6PRu$) = 812.15 g mol^{-1}; anal. calcd for $C_{37}H_{30}N_4ClF_6PRu$: C 54.72, H 3.72, N 6.90; found: C 54.44; H 3.41; N 6.51; Mp: 172–174 °C; R_f (100% methanol): 0.81; Mp: >300 °C; R_f (pure methanol): 0.85; IR (cm^{-1}): ν sp^3 C–H stretching (3048), Ar C=C stretching (1618), C–N stretching (1433), sp^3 C–H bending (1414), P–F stretching (831), C–H bending (556); ^{1}H NMR (DMSO-d_6, 400 MHz): δ 0.96 (d, 6H, J = 6.8 Hz, H-i, H-j, cymene isopropyl–CH$_3$); 2.23 (s, 3H, H-a, cymene CH$_3$); 2.63–2.70 (m, 1H, H-h, cymene C–H); 6.14 (d, 2H, J = 6.0 Hz, H-e, H-f, cymene ArH); 6.39 (d, 2H, J = 6.0 Hz, H-c, H-d, cymene ArH); 7.53 (d, 2H, H-23, J = 6.4 Hz, H-19, ArH); 7.62 (t, 3H, J = 7.4 Hz, H-17, H-18, H-24, ArH); 7.77 (d, 2H, J = 8.4 Hz, H-16, H-26, ArH); 8.22 (t, 2H, J = 6.4 Hz, H-2, H-9, ArH); 8.27 (d, 3H, J = 8.8 Hz, H-3, H-8, H-25, ArH); 8.95 (s, 1H, H-21, ArH); 9.91 (d, 2H, J = 5.2 Hz, H-1, H-10, ArH); ^{13}C NMR (DMSO-d_6, 100 MHz): δ 18.8 (Me, C-a, *p*-cymene), 21.9 (Me, C-i, *p*-cymene), 22.1 (Me, C-j, *p*-cymene), 30.9 (CH, C-h, *p*-cymene), 84.4 (ArCH, C-f, *p*-cymene), 85.9 (ArCH, C-e, *p*-cymene), 86.7 (ArCH, C-d, *p*-cymene), 86.8 (ArCH, C-c, *p*-cymene), 103.7 (ArC, C-g, *p*-cymene), 104.7 (ArC, C-b, *p*-cymene), 124.8 (2C, C-2, C-9), 125.9 (1C, C-12), 126.3 (2C, C-16, C-26), 126.9 (2C, C-20, C-22), 129.1 (3C, C-11, C-15, C-27), 130.1 (6C, C-4, C-7, C-17, C-18, C-24, C-25), 131.1 (2C, C-19, C-23), 131.3 (3C, C-3, C-8, C-21), 132.9 (1C, C-14), 139.8 (1C, C-5), 143.9 (2C, C-1, C-10), 151.2 (1C, C-13), 154.4 (1C, C-6); ^{19}F NMR (DMSO-d_6, 376 MHz): δ −71.07 to −69.18 (6F, PF_6); ^{31}P NMR (DMSO-d_6, 162 MHz): δ −157.4 to −131.04 (PF_6); ESI-MS (MeOH): m/z = 667.0 [M]$^+$.

*[(η^6-p-Cymene)Ru^{II}Cl{K^2-N,N-(3-(1H-imidazo[4,5-f][1,10]phenanthrolin-2-yl)-4H-chromen-4-one)}]PF$_6$ (**RuL2**).* 45 mg (0.060 mmol, 92%); Mr ($C_{32}H_{26}N_4O_2ClF_6PRu$) = 780.06 g mol^{-1}; anal. calcd for $C_{32}H_{26}N_4ClF_6PRu$: C 49.27, H 3.36, N 7.18; found: C 49.56; H 3.14; N 7.48; Mp: >300 °C; R_f (pure methanol): 0.78; IR (cm^{-1}): ν sp^3 C–H stretching (3050), Ar C=C stretching (1641), C–N stretching (1464), sp^3 C–H bending (1408), P–F stretching (833), C–H bending (556); ^{1}H NMR (DMSO-d_6, 400 MHz): δ 0.91(d, 6H, J = 7.2 Hz, H-i, H-j, cymene isopropyl–CH$_3$); 2.21 (s, 3H, H-a, cymene CH$_3$); 2.57–2.64 (m, 1H, H-h, cymene C–H); 6.13 (d, 2H, J = 6.0 Hz, H-e, H-f, cymene ArH); 6.34 (d, 2H, J = 6.4 Hz, H-c, H-d, cymene ArH); 7.66 (t, 2H, J = 7.6 Hz, H-2, H-9, ArH); 7.84 (d, 1H, J = 8.4 Hz, H-3, ArH); 7.94 (t, 1H, J = 8 Hz, H-8, ArH); 8.19–8.23 (m, 3H, H-18, H-19, H-20, ArH); 8.30 (d, 1H, J = 7.6 Hz, H-17, ArH); 9.39 (s, 1H, H-15, ArH); 9.88 (d, 2H, J = 5.2 Hz, H-1, H-10, ArH); ^{13}C NMR (DMSO-d_6, 100 MHz): δ 18.8 (Me, C-a, *p*-cymene), 21.9 (Me, C-i, *p*-cymene), 22.0 (Me, C-j, *p*-cymene), 30.9 (CH, C-h, *p*-cymene), 84.3 (ArCH, C-f, *p*-cymene), 85.9 (ArCH, C-e, *p*-cymene), 86.7 (ArCH, C-d, *p*-cymene), 86.8 (ArCH, C-c, *p*-cymene), 100.6 (ArC, C-b, *p*-cymene), 103.7 (ArC, C-g, *p*-cymene), 104.3 (1C, C-15), 114.8 (1C, C-20), 119.2 (2C, C-2, C-9), 123.7 (2C, C-11, C-18), 125.7 (2C, C-12, C-21), 126.8 (2C, C-4, C-17), 127.0 (1C, C-7), 133.1 (1C, C-8), 135.6 (1C, C-8), 143.6 (1C, C-13), 147.0 (2C, C-1, C-10), 154.3 (2C, C-5, C-19), 156.0 (2C, C-6, C-22), 159.0 (1C, C-14), 174.8 (1C, C-16); ^{19}F NMR (DMSO-d_6, 376 MHz): δ −71.08 to −69.19 (6F, PF_6); ^{31}P NMR (DMSO-d_6, 162 MHz): δ −157.36 (PF_6), δ −152.97 to −131.03 (PF_6); ESI-MS (MeOH): m/z = 635.9 [M]$^+$.

*[(η^6-p-Cymene)Ru^{II}Cl{K^2-N,N-(2-(1H-indol-3-yl)-1H-imidazo[4,5-f][1,10]phenanthroline)}]PF$_6$ (**RuL3**).* 46.1 mg (0.0614 mmol, 94%); Mr ($C_{31}H_{27}N_5ClF_6PRu$) = 751.07 g mol^{-1}; anal. calcd for

$C_{31}H_{27}N_5ClF_6PRu$: C 49.57, H 3.62, N 9.32; found: C 49.76; H 3.14; N 9.58; Mp: >300 °C; R_f (pure methanol): 0.80; IR (cm^{-1}): ν sp^3 C–H stretching (3418), Ar C=C stretching (1587), sp^3 C–H bending (1449), C–N stretching (1368), P–F stretching (831), C–H bending (554); ^{1}H NMR (DMSO-d_6, 400 MHz): δ 0.91 (d, 6H, H–I, H-j, J = 6.0 Hz, cymene isopropyl–CH_3); 2.20 (s, 3H, H-a, cymene CH_3); 2.58–2.66 (m, 1H, H-h, cymene C–H); 6.11 (d, 2H, J = 6 Hz, H-e, H-f, cymene ArH); 6.34 (d, 2H, J = 6.0 Hz, H-c, H-d, cymene ArH); 7.25–7.28 (m, 4H, H-3, H-8, H-16, H-19, ArH); 7.55 (t, 1H, J = 5.6 Hz, H-17, ArH); 8.16–8.20 (m, 2H, H-2, H-9, ArH); 8.68 (t, 1H, J = 4.4 Hz, H-18, ArH); 8.55 (s, 1H, imidazole NH-proton); 9.37 (d, 1H, J = 5.6 Hz, H-14, ArH); 9.83 (d, 2H, J = 5.2 Hz, H-1, H-10, ArH); 11.8 (s, 1H, indole NH-proton); ^{13}C NMR (DMSO-d_6, 100 MHz): δ 18.8 (Me, C-a, *p*-cymene), 21.9 (Me, C-i, *p*-cymene), 22.1 (Me, C-j, *p*-cymene), 30.4 (CH, C-h, *p*-cymene), 84.3 (ArCH, C-c, *p*-cymene), 85.9 (ArCH, C-d, *p*-cymene), 86.7 (ArCH, C-e, *p*-cymene), 86.8 (ArCH, C-f, *p*-cymene), 100.6 (ArC, C-b, *p*-cymene), 103.6 (ArC, C-g, *p*-cymene), 104.2 (1C, C-15), 106.4 (1C, C-19), 106.9 (1C, C-17), 112.6 (4C, C-16, C-18, C-2, C-9), 114.0 (2C, C-11, C-12), 121.1 (2C, C-20, C-7), 121.8 (2C, C-4, C-14), 123.1(1C, C-3), 125.6 (1C, C-8), 127.2 (1C, C-5), 132.7 (1C, C-21), 137.0 (2C, C-1, C-10), 151.6 (2C, C-6, C-13); ^{19}F NMR (DMSO-d_6, 376 MHz): δ −71.10 to −69.21 (6F, PF_6); ^{31}P NMR (DMSO-d_6, 162 MHz): δ −157.35 to −131.02 (PF_6); ESI-MS (MeOH): m/z = 606.4 $[M]^+$.

*[(η^6-p-Cymene)Ru^{II}Cl{K^2-N,N-(2-(naphthalene-1-yl)-1H-imidazo[4,5-f][1,10]phenanthroline)}]PF_6 (**RuL4**).* 47.2 mg (0.062 mmol, 95%); Mr ($C_{33}H_{28}N_4ClF_6PRu$) = 762.09 g mol^{-1}; anal. calcd for $C_{33}H_{28}N_4ClF_6PRu$: C 52.01, H 3.70, N 7.35; found: C 52.46; H 3.74; N 7.68; Mp: >300 °C; R_f (pure methanol): 0.82; IR (cm^{-1}): ν N–H stretching (3615), sp^3 C–H stretching (3051), Ar C=C stretching (1620), C–N stretching (1443), sp^3 C–H bending (1408), P–F stretching (835), C–H bending (556); ^{1}H NMR (DMSO-d_6, 400 MHz): δ 0.90 (d, 6H, J = 6.8 Hz, H-i, H-j, cymene isopropyl–CH_3); 2.22 (s, 3H, H-a, cymene CH_3); 2.77–2.84 (m, 1H, H-h, cymene C–H); 5.75 (d, 1H, J = 6.4 Hz, H-f, ArH); 5.80 (d, 1H, J = 6.4 Hz, H-e, ArH); 6.10 (d, 1H, J = 6.4 Hz, H-d, cymene ArH); 6.34 (d, 1H, J = 6.0 Hz, H-c, cymene ArH); 7.62–7.69 (m, 2H, H-2, H-9, ArH); 7.74 (t, 1H, J = 7.6 Hz, H-18, ArH); 8.08 (d, 1H, J = 7.2 Hz, H-17, ArH); 8.11–8.17 (m, 2H, H-15, H-21, ArH); 8.19–8.22 (m, 3H, H-16, H-19, H-20, ArH); 8.95 (d, 1H, J = 8 Hz, NH-proton); 9.27 (d, 2H, J = 8.0 Hz, H-3, H-8, ArH); 9.85 (d, 2H, J = 4.8 Hz, H-1, H-10, ArH); ^{13}C NMR (DMSO-d_6, 100 MHz): δ 18.3 (Me, C-a, *p*-cymene), 21.9 (Me, C-i, *p*-cymene), 22.1 (Me, C-j, *p*-cymene), 30.9 (CH, C-h, *p*-cymene), 84.2 (ArCH, C-f, *p*-cymene), 85.9 (ArCH, C-e, *p*-cymene), 86.8 (ArCH, C-c, C-d, *p*-cymene), 100.7 (ArCH, C-g, *p*-cymene), 103.9 (ArCH, C-b, *p*-cymene), 107.0 (2C, C-2, C-9), 125.8 (1C, C-11), 126.3 (1C, C-12), 126.8 (3C, C-7, C-15, C-16), 127.0 (3C, C-4, C-19, C-20), 127.1 (2C, C-17, C-18), 127.9 (1C, C-17, C-21), 128.9 (2C, C-22, C-23), 130.8 (1C, C-3), 131.3 (1C, C-8), 133.0 (1C, C-5), 134.0 (1C, C-14) 143.6 (2C, C-1, C-10), 153.2 (1C, C-13), 154.3 (1C, C-6); ^{19}F NMR (DMSO-d_6, 376 MHz): δ −71.08 to −69.21 (6F, PF_6); ^{31}P NMR (DMSO-d_6, 162 MHz): δ −157.37 to −131.02 (PF_6); ESI-MS (MeOH): m/z = 617.4 $[M]^+$.

In vitro cytotoxic study, cellular uptake and imaging study

In vitro cytotoxicity was evaluated using the typical MTT assay protocol.[65] The synthesized complexes (**RuL1–RuL4**) were dissolved in 0.1% DMSO and then serially diluted with DMEM medium. Two cancer cell lines, *i.e.* human epithelioid cervix carcinoma (HeLa), human epithelial colorectal adenocarcinoma cells (Caco-2), and one normal kidney cell line (HEK 293) were used in this assay. Approximately 1×10^4 cells per well were cultured in 100 μL of growth medium in 96-well plates and incubated at 37 °C under a 5% CO_2 atmosphere. The cells were then treated with different concentrations of the drugs (2.45–300 μM for HeLa cell and 0.78–100 μM for CaCo-2 cells) in the volume of 100 μM per well. Cisplatin was used as a standard positive control drug. The cells in the control wells also received the same volume of medium containing 0.1% DMSO. After 48 h (for HeLa)/72 h (for Caco-2), the medium was superfluous and cell cultures were incubated with 100 μL MTT reagent (1 mg mL^{-1}) for 5 h at 37 °C. Then the suspension was placed on a micro-vibrator for 10 min followed by recording the absorbance at λ = 570 nm using an ELISA reader. A similar experiment was performed in excess GSH (1 mM) and hypoxic condition (1% O_2). The experiment was also performed in triplicate. The data is presented as the growth inhibition percentage, *i.e.* % growth inhibition = 100 − [(AD × 100)/AB], where AD is the measured absorbance in the wells containing the samples and AB is the measured absorbance for the blank wells (cells with a medium and a vehicle).

Cellular localization of RuL1 using nuclear staining dye DAPI (4′,6-diamidino-2-phenylindole dihydrochloride)

To study the cellular uptake of **RuL1**, briefly HeLa cells (1×10^4 cells per well) were plated on 12-well plates and allowed to adhere for 4–8 hours. The cells were then incubated with 20 μM of complex **RuL1** in complete DMEM medium for 4 h at 37 °C. Thereafter, the cells were washed 3 times with 1× PBS at room temperature. The cells were counterstained with 5 μg mL^{-1} of DAPI at room temperature in the dark for 5 min. After gentle washing in 10× PBS 3 times, the cells were viewed under a confocal microscope using the respective filter.

Estimation of cellular Ru content by ICP-MS analysis

Quantification of the total ruthenium uptake was performed with HeLa cells by ICP-MS analysis. Around 10^6 cells were seeded in a 10 cm tissue culture Petri dish and then grown for 48 h in DMEM media. Subsequently, the cells were treated with fresh DMEM/DMSO media (pH 7.4, 1 : 99, v/v) containing **RuL1–RuL4** and RAPTA-C (5 μM) for another 24 h. The treated cells were washed and pelleted by centrifugation at 10 000 rpm for 10 min at 4 °C. The pelleted cells were then collected and left to air dry for 5 min. Subsequently, the dry pellets were treated with ultra-pure grade 65% HNO_3 (Sigma) at 65 °C on a water bath for 8 h. Each sample was diluted to 10 mL with Milli-Q water containing 2% HNO_3 solution. The samples were analysed using a Thermo Scientific XSERIES-2 ICP-MS instrument for ruthenium content spiked with an internal standard,

indium. Untreated HeLa cell controls were included for analysis; however, the ruthenium content in these samples was observed to be below the detection limits of the instrument. All data obtained were subsequently subtracted from the blank sample data (2% HNO_3 in Milli-Q water). Sample data fitting was performed using the standard curve drawn with different concentrations (10–200 ppb) of the standard ruthenium sample. Ruthenium content was expressed as nmol per 10^6 cells. Triplicate experiments were performed to calculate the standard deviation of the data.

Stability study

The stability of two Ru(II) complexes (**RuL1** and **RuL4**) were tested in aqueous DMSO (H_2O : DMSO = 9 : 1) and GSH medium.

Viscosity measurement

To determine the binding mode of the drugs, using compound **RuL4** and EtBr treated DNA, a hydrodynamic method, namely a viscosity study, was conducted using an Ostwald Viscometer.

DNA binding study

The binding of the complexes with calf-thymus DNA (CT-DNA) was observed by electronic spectra and competitive binding assay using ethidium bromide (EtBr) as the quencher by fluorescence spectroscopy.

UV–visible studies

The DNA binding assay was carried out using complexes **RuL1** and **RuL4** in Tris-HCl buffer (5 mM Tris-HCl in water, pH 7.4) in water medium.[66] The concentration of CT-DNA was calculated from its absorbance intensity at 260 nm and its known molar absorption coefficient value of 6600 M^{-1} cm^{-1}. An equal amount of DNA was added to in the sample and reference in cuvettes. The titration was carried out by increasing the concentration of CT-DNA. Before each measurement, the sample was equilibrated with CT-DNA for about 5 min, and then the absorbance of the complex was measured. The intrinsic DNA binding constant (K_b) was calculated using eqn (i) as follows:

$$\frac{[\mathrm{DNA}]}{(\varepsilon_a - \varepsilon_f)} = \frac{[\mathrm{DNA}]}{(\varepsilon_b - \varepsilon_f)} + \frac{1}{K_b(\varepsilon_a - \varepsilon_f)} \quad \text{(i)}$$

where [DNA] is the concentration of DNA in the base pairs, ε_a is the apparent extinction coefficient observed for the complex, ε_f corresponds to the extinction coefficient of the complex in its free form, and ε_b refers to the extinction coefficient of the complex when fully bound to DNA. The data was plotted using Origin Lab, version 8.5 to obtain the $[DNA]/(\varepsilon_a - \varepsilon_f)$ *vs.* [DNA] linear plot. The ratio of the slope to intercept from the linear fit gives the value of the intrinsic binding constant (K_b).

UV-vis and fluorescence study

The UV-vis and fluorescence study of all the Ru(II)complexes was performed in 10% DMSO solution. The fluorescence quantum yields (Φ) were calculated using the comparative William's method, which involves the use of a well-characterized standard with a known quantum yield value using 10% DMSO solution.[67] Quinine sulphate is generally used as the standard. The quantum yield was calculated according to eqn (ii) as follows:

$$\varphi = \varphi_R \times \frac{I_S}{I_R} \times \frac{OD_R}{OD_S} \times \frac{\eta_S}{\eta_R} \quad \text{(ii)}$$

where φ = quantum yield, I = peak area, OD = absorbance at λ_{max}, η = refractive index of solvent (S) and reference (R). Here, we used quinine sulphate as the standard for calculating the quantum yield.

Ethidium bromide displacement assay

The ethidium bromide (EtBr) displacement assay was carried out to explain the mode of binding between the potent compounds with DNA.[68] The apparent binding constant (K_{app}) of complexes **RuL1** and **RuL4** to CT-DNA was calculated using ethidium bromide (EtBr) as a spectral probe in 5 mM Tris-HCl buffer (pH 7.4). The values of the apparent binding constant (K_{app}) were obtained using eqn (iii):

$$K_{app} \times [\mathrm{complex}]_{50} = k_{EtBr} \times [\mathrm{EtBr}] \quad \text{(iii)}$$

where K_{EtBr} is the EtBr binding constant (K_{EtBr} = 1.0 × 10^7 M^{-1}), and [EtBr] = 8 × 10^{-6} M. The Stern–Volmer equation was employed for the quantitative determination of the Stern–Volmer quenching constant (K_{SV}).[69] The Origin (8.5) software was used to plot the fluorescence data to obtain the linear plot of I_0/I *vs.* [complex]. The value of K_{SV} was calculated using the following equation.

$$I_0/I = 1 + K_{SV}\,[Q] \quad \text{(iv)}$$

where I_0 = fluorescence intensity in the absence of the complex and I = fluorescence intensities in the presence of the complex of concentration [Q].

Protein binding studies

Serum albumin proteins are major components in blood plasma proteins and play significant roles in drug transport and metabolism.[70] The interaction of the drug with bovine serum albumin (BSA), a structural homologue with human serum albumin (HSA), was studied using a tryptophan emission quenching experiment. The tryptophan emission quenching experiment was performed to detect the interaction of the ruthenium complex **RuL1** and **RuL4** with the BSA protein. Initially, BSA solution (2 × 10^{-6} M) was prepared in Tris-HCl/NaCl buffer. Aqueous solutions of the complexes with increasing concentrations were subsequently added to the BSA solution. After each addition, the solutions were shaken slowly for 5 min before recording the fluorescence at a wavelength of 295 nm (λ_{ex} = 295 nm). A gradual decrease in the fluorescence intensity of BSA at λ = 340 nm was observed upon increasing the concentration of the complex, which confirmed that the interaction between the complex and BSA occurred. The Stern–Volmer equation was employed to quantitatively determine the

quenching constant (K_{BSA}). Origin Lab, version 8.5 was used to plot the emission spectral data to obtain the linear plot of I_0/I *vs.* [complex] using eqn (v) as follows:

$$I_0/I = 1 + K_{BSA}\,[Q] = 1 + k_q\tau_0\,[Q] \quad \text{(v)}$$

where I_0 is the fluorescence intensity of BSA in the absence of the complex and I is the fluorescence intensity of BSA in the presence of the complex of concentration [Q], τ_0 = lifetime of the tryptophan in BSA, which was determined to be 1×10^{-8}, and k_q is the quenching constant. Scatchard eqn (vi) gives the binding properties of the complexes,[71] where K = binding constant and n = number of binding sites.

$$\log(I_0 - I/I) = \log K + n \log\,[Q] \quad \text{(vi)}$$

Conductivity measurement

To confirm the interaction of the complexes with water, DMSO, GSH and CT-DNA solutions, the conductivity of the prepared complexes were determined using a conductivity-TDS Meter-307 (Systronics, India) and cell constant of 1.0 cm^{-1}.[72] The change in conductivity was also measured in different pH media. Time-dependent conductivity measurements were also performed.

n-Octanol–water partition coefficient (log *P*)

The log *P* of the ruthenium complexes were determined *via* the shake flask method using the previously published procedure.[49] A known amount of each complex (**RuL1–RuL4**) was suspended in water (pre-saturated with *n*-octanol) and shaken for 48 h on an orbital shaker. To allow phase separation, the solution was centrifuged for 10 min at 3000 rpm. Then the amount of ruthenium present in the saturated aqueous solution was measured by ICP-MS. To obtain the partition coefficient, different ratios (0.5 : 1, 1 : 1, and 2 : 1) of the saturated solutions were shaken with pre-saturated *n*-octanol for 20 min on an orbital shaker following the same procedure.

Statistical analysis

All the IC_{50} data are presented as the mean ± standard deviation. The results are the mean of three independent experiments carried out in each cell line, where in each experiment, each concentration was assayed in triplicate. The statistical analyses were performed using the Origin 8.5 software and Student's *t*-test.

Conclusions

In summary, we meticulously synthesized ruthenium(II)-*p*-cymene-2-arylimidazophenanthroline scaffolds under sonication and evaluated their potential as potent anticancer agents. The quantum yield values indicated that the complexes are moderately fluorescent, with the anthracene derivative (**RuL1**) showing the best quantum yield. The stability studies indicated that the complexes formed a Ru(II)–arene(H_2O)(N^N) bi-cationic system, which was fairly stable, and thus facilitated covalent binding with DNA. All the DNA binding studies revealed that the complexes bound efficiently to DNA through intercalation, which can be attributed to the fact that the two complexes studied were highly planar due to their enhanced conjugation. The viscosity results also supported the intercalation and covalent binding mode of these complexes with DNA, which ensured the increased scope of their binding ability. However, the BSA binding study demonstrated the higher binding capacity of **RuL1** in comparison to that of **RuL4**. In addition, the cytotoxicity data revealed the very high potency and selectivity of **RuL4** in two cell lines compared to that of cisplatin and RAPTA-C. The complexes also showed an insignificant change in cytotoxicity in the presence of a high GSH concentration and hypoxic conditions compared to normoxia, which indicated the importance of serum albumin for combating GSH, stopping the deactivation process. Furthermore, complex **RuL4** exhibited more effective cytotoxicity against the hypoxic cancer cells than cisplatin. In addition, complex **RuL1** is a highly promising theranostic agent based on its MLCT fluorescence efficiency and high cellular uptake, inducing appreciable cytoselectivity in HeLa cells together with high cellular imaging property.

Conflicts of interest

There are no conflicts to declare.

Acknowledgements

The authors are grateful to VIT for 'VIT SEED GRANT'. We acknowledge DST, New Delhi, India for DST-FIST project. We also acknowledge to Department of Science and Technology, Government of India for supporting the work through the DST-EMR project grant (EMR/2017/000816).

Notes and references

1 M. Heron, *Natl. Vital Stat. Rep.*, 2013, **62**, 1–97.
2 R. J. McQuitty, *Sci. Prog.*, 2014, **97**, 1–19.
3 L. H. Hurley, *Nat. Rev. Cancer*, 2002, **2**, 188–200.
4 Md. Hanif and C. G. Hartinger, *Future Med. Chem.*, 2018, **10**, 615–617.
5 U. Ndagi, Nd. Mhlongo and M. E. Soliman, *Drug Des., Dev. Ther.*, 2017, **11**, 599–616.
6 E. Lamour, S. Routier, J.-L. Bernier, J.-P. Catteau, C. Bailly and H. Vezin, *J. Am. Chem. Soc.*, 1999, **121**, 1862–1869.
7 A. Naik, R. Rubbiani, G. Gasser and B. Spingler, *Angew. Chem., Int. Ed.*, 2014, **53**, 6938–6941.
8 T. Zou, J. Liu, C. T. Lum, C. Ma, R. C.-T. Chan, C.-N. Lok, W.-M. Kwok and C.-M. Che, *Angew. Chem., Int. Ed.*, 2014, **53**, 10119–10123.
9 J.-J. Zhang, W. Lu, R. W.-Y. Sun and C.-M. Che, *Angew. Chem., Int. Ed.*, 2012, **51**, 4882–4886.

10 K. Suntharalingam, S. G. Awuah, P. M. Bruno, T. C. Johnstone, F. Wang, W. Lin, Y. R. Zheng, J. E. Page, M. T. Hemann and S. J. Lippard, *J. Am. Chem. Soc.*, 2015, **137**, 2967–2974.
11 K. Suntharalingam, W. Lin, T. C. Johnstone, P. M. Bruno, Y. R. Zheng, M. T. Hemann and S. J. Lippard, *J. Am. Chem. Soc.*, 2014, **136**, 14413–14416.
12 D. L. Ma, D. S. Chan and C. H. Leung, *Acc. Chem. Res.*, 2014, **47**, 3614–3631.
13 Z. Li, A. David, B. A. Albani, J. P. Pellois, C. Tur and K. R. Dunbar, *J. Am. Chem. Soc.*, 2014, **136**, 17058–17070.
14 (*a*) E. Alessio, *Eur. J. Inorg. Chem.*, 2017, **2017**, 1549–1560; (*b*) G.-B. Jiang, W.-Y. Zhang, M. He, Y.-Y. Gu, L. Bai, Y.-J. Wang, Q.-Y. Yi and F. Du, *Spectrochim. Acta, Part A*, 2020, **227**, 117534; (*c*) G.-B. Jiang, W.-Y. Zhang, M. He, Y.-Y. Gu, L. Bai, Y.-J. Wang, Q.-Y. Yi and F. Du, *J. Inorg. Biochem.*, 2020, **208**, 111104.
15 I. Kostova, *Curr. Med. Chem.*, 2006, **13**, 1085–1107.
16 C. Artner, H. U. Holtkamp, C. G. Hartinger and S. M. Meier-Menches, *J. Inorg. Biochem.*, 2017, **177**, 322–327.
17 (*a*) G. R. Jadhav, S. Sinha, M. Chhabra and P. Paira, *Bioorg. Med. Chem. Lett.*, 2016, **26**, 2695–2700; (*b*) R. G. Kenny and C. J. Marmion, *Chem. Rev.*, 2019, **119**, 1058–1137; (*c*) R. Trondl, P. Heffeter, C. R. Kowol, M. A. Jakupec, W. Berger and B. K. Keppler, *Chem. Sci.*, 2014, **5**, 2925–2932; (*d*) W.-H. Ang, A. Casini, G. Sava and P. J. Dyson, *J. Organomet. Chem.*, 2011, **696**, 989–998.
18 N. Muhammad and Z. Guo, *Curr. Opin. Chem. Biol.*, 2014, **19**, 144–153.
19 (*a*) F. Kratz and B. Elsadek, *J. Controlled Release*, 2012, **161**, 429–445; (*b*) M. Groessl, E. Reisner, C. G. Hartinger, R. Eichinger, O. Semenova, A. R. Timerbaev, M. A. Jakupec, V. B. Arion and B. K. Keppler, *J. Med. Chem.*, 2007, **50**, 2185–2193.
20 A. Bergamo, L. Messori, F. Piccioli, M. Cocchietto and G. Sava, *Invest. New Drugs*, 2003, **21**, 401–411.
21 E. Alessio, G. Mestroni, A. Bergamo and G. Sava, *Curr. Top. Med. Chem.*, 2004, **4**, 1525–1535.
22 C. G. Hartinger, M. A. Jakupec, S. Zorbas-Seifried, M. Groessl, A. Egger, W. Berger, H. Zorbas, P. J. Dyson and B. K. Keppler, *Biodiversity*, 2008, **5**, 2140–2155.
23 C. G. Hartinger, S. Zorbas-Seifried, M. A. Jakupec, B. Kynast, H. Zorbas and B. K. Keppler, *J. Inorg. Biochem.*, 2006, **100**, 891–904.
24 L. Zeng, P. Gupta, Y. Chen, E. Wang, L. Ji, H. Chao and Z. S. Chen, *Chem. Soc. Rev.*, 2017, **46**, 5771–5804.
25 D. A. Smithen, H. Yin, M. H. R. Beh, M. Hetu, T. S. Cameron, S. A. McFarland and A. Thompson, *Inorg. Chem.*, 2017, **56**, 4121–4132.
26 P. J. Dyson, *Chimia*, 2007, **61**, 698–670.
27 J. M. Rademaker-Lakhai, D. van den Bongard, D. Pluim, J. H. Beijnen and J. H. M. A. Schellens, *Clin. Cancer Res.*, 2004, **10**, 3717–3727.
28 R. Carter, A. Westhorpe, M. J. Romero, A. Habtemariam, C. R. Gallevo, Y. Bark, N. Menezes, P. J. Sadler and R. A. Sharma, *Sci. Rep.*, 2016, **6**, 20596.
29 E. A. Hillard, A. Vessières and J. Jaouen, *Top. Organomet. Chem.*, 2010, **32**, 81–117.
30 (*a*) M. J. Clarke, *Coord. Chem. Rev.*, 2003, **236**, 209–233; (*b*) S. Brown, M. Georgatos, C. Reifel, J. H. Song, S. H. Shin and M. Hong, *Endocrine*, 2002, **18**, 91–96.
31 (*a*) A. M. Pizarro, A. Habtemariam and P. J. Sadler, *Top. Organomet. Chem.*, 2010, **32**, 21–56; (*b*) M. A. Jakupec, M. Galanski, V. B. Arion, C. G. Hartinger and B. K. Keppler, *Dalton Trans.*, 2008, 183–194; (*c*) F. Wang, A. Habtemariam, E. P. L. van der Geer, R. Fernandez, M. Melchart, R. J. Deeth, R. Aird, S. Guichard, F. P. A. Fabbiani, P. Lozano-Casal, I. D. H. Oswald, D. I. Jodrell, S. Parsons and P. J. Sadler, *Proc. Natl. Acad. Sci. U. S. A.*, 2005, **102**, 18269–18274.
32 (*a*) F. Wang, H. Chen, J. A. Parkinson, P. D. S. Murdoch and P. J. Sadler, *Inorg. Chem.*, 2002, **41**, 4509–4523; (*b*) F. Wang, J. Xu, A. Habtemariam, J. Bella and P. J. Sadler, *J. Am. Chem. Soc.*, 2005, **127**, 17734–17743; (*c*) M. A. Fuertes, C. Alonso and J. M. Perez, *Chem. Rev.*, 2003, **103**, 645–662; (*d*) S. Tsuchida and K. Sato, *Crit. Rev. Biochem. Mol. Biol.*, 1992, **27**, 337–384.
33 (*a*) L. A. Ralat and R. F. Colman, *J. Biol. Chem.*, 2004, **279**, 50204–50213; (*b*) C. C. McIlwain, D. M. Townsend and K. D. Tew, *Oncogene*, 2006, **25**, 1639–1648; (*c*) K. D. Tew, *Cancer Res.*, 1994, **54**, 4313–4320; (*d*) S. J. Dougan, A. Habtemariam, S. E. McHale, S. Parsons and P. J. Sadler, *Proc. Natl. Acad. Sci. U. S. A.*, 2008, **105**, 11628–11633; (*e*) F. Wang, J. Xu, K. Wu, S. K. Weidt, C. L. MacKay, P. R. R. Langridge-Smith and P. J. Sadler, *Dalton Trans.*, 2013, **42**, 3188–3195.
34 (*a*) Z. Almodares, S. J. Lucas, B. D. Crossley, A. M. Basri, C. M. Pask, A. J. Hebden, R. M. Phillips and P. C. McGowan, *Inorg. Chem.*, 2014, **53**, 727–736; (*b*) S. Koch, F. Mayer, F. Honecker, M. Schittenhelm and C. Bokemeyer, *Br. J. Cancer*, 2003, **89**, 2133–2139.
35 (*a*) A. Habtemariam, M. Melchart, R. Fernandez, S. Parsons, I. D. H. Oswald, A. Parkin, F. P. A. Fabbiani, J. E. Davidson, A. Dawson, R. E. Aird, D. I. Jodrell and P. J. Sadler, *J. Med. Chem.*, 2006, **49**, 6858–6868; (*b*) R. E. Aird, J. Cummings, A. A. Ritchie, M. Muir, R. E. Morris, H. Chen, P. J. Sadler and D. I. Jodrell, *Br. J. Cancer*, 2002, **86**, 1652–1657.
36 (*a*) W. Kandioller, C. G. Hartinger, A. A. Nazarov, C. Bartel, M. Skocic, M. A. Jakupec, V. B. Arion and B. K. Keppler, *Chem. – Eur. J.*, 2009, **15**, 12283–12291; (*b*) S. J. Dougan, M. Melchart, A. Habtemariam, S. Parsons and P. J. Sadler, *Inorg. Chem.*, 2006, **45**, 10882–10894; (*c*) S. Betanzos-Lara, O. Novakova, R. J. Deeth, A. M. Pizarro, G. J. Clarkson, B. Liskova, V. Brabec, P. J. Sadler and A. Habtemariam, *J. Biol. Inorg. Chem.*, 2012, **17**, 1033–1051.
37 A. Bencini and V. Lippolis, *Coord. Chem. Rev.*, 2010, **254**, 2096–2180.
38 E. R. Jamieson and S. J. Lippard, *Chem. Rev.*, 1999, **99**, 2467–2498.
39 M. A. Jakupec, M. Galanski, V. B. Arion, C. G. Hartinger and B. K. Keppler, *Dalton Trans.*, 2008, 183–194.

40 G. S. Smith and B. Therrien, *Dalton Trans.*, 2011, **40**, 10793–10800.
41 L. Gök and H. Türkmen, *Tetrahedron*, 2013, **69**, 10669–10674.
42 S. Nikolić, L. Rangasamy, N. Gligorijević, S. Aranđelović, S. Radulović, G. Gasser and S. Grgurić-Šipka, *J. Inorg. Biochem.*, 2016, **160**, 156–165.
43 Q. Wu, C. Fan, T. Chen, C. Liu, W. Mei, S. Chen, B. Wang, Y. Chen and W. Zheng, *Eur. J. Med. Chem.*, 2013, **63**, 57–63.
44 C. Gaiddon, P. Jeannequin, P. Bischoff, M. Pfeffer, C. Sirlin and J. P. Loeffler, *J. Pharmacol. Exp. Ther.*, 2005, **315**, 1403–1411.
45 G.-L. Gan, H. Chao, S.-B. Ji, L.-L. Chen and H. Li, *Spectrochim. Acta, Part A*, 2012, **97**, 297–305.
46 (*a*) S. K. Subran, S. Banerjee, A. Mondal and P. Paira, *New J. Chem.*, 2016, **40**, 10333–10343; (*b*) A. Mondal, S. De, S. Maiti, B. Sarkar, A. K. Sk, R. Jacob, A. Moorthy and P. Paira, *J. Photochem. Photobiol., B*, 2018, **178**, 380–394; (*c*) S. De, S. RayChaudhuri, A. Panda, G. R. Jadhav, R. S. Kumar, P. Manohar, N. Ramesh, A. Mondal, A. Moorthy, S. Banerjee, P. Paira and A. K. Sk, *New J. Chem.*, 2019, **43**, 3291–3302; (*d*) B. Sarkar, A. Mondal, Y. Madaan, N. Roy, A. Moorthy, Y.-C. Kuo and P. Paira, *Dalton Trans.*, 2019, **48**, 12257–12271.
47 Y. Chen, L. Qiao, L. Ji and H. Chao, *Biomaterials*, 2014, **35**, 2–13.
48 C. Jin, J. Liu, Y. Chen, L. Zeng, R. Guan, C. Ouyang, L. Ji and H. Chao, *Chem. – Eur. J.*, 2015, **21**, 12000–12010.
49 M. Kubanik, H. Holtkamp, T. Söhnel, S. M. F. Jamieson and C. G. Hartinger, *Organometallics*, 2015, **34**, 5658–5668.
50 (*a*) M. Sunita, B. Anupama, B. Ushaiah and C. GyanaKumari, *Arabian J. Chem.*, 2017, **10**, S3367–S3374; (*b*) W. J. Geary, *Coord. Chem. Rev.*, 1971, **7**, 81–122; (*c*) I. Ali, W. A. Wani and K. Saleem, *Synth. React. Inorg., Met.-Org., Nano-Met. Chem.*, 2013, **43**, 1162–1170.
51 (*a*) S. Bhattacharyya, K. Purkait and A. Mukherjee, *Dalton Trans.*, 2017, **46**, 8539; (*b*) K. Purkait, S. Karmakar, S. Bhattacharyya, S. Chatterjee, S. K. Dey and A. Mukherjee, *Dalton Trans.*, 2015, **44**, 5969–5973.
52 D. M. Townsend and K. D. Tew, *Oncogene*, 2003, **22**, 7369–7375.
53 B. G. Campling, K. Baer, H. M. Baker, Y. M. Lam and S. P. Cole, *Br. J. Cancer*, 1993, **68**, 327–335.
54 N. Shahabadi, S. Kashanian, M. Mahdavi and N. Sourinejad, *Bioinorg. Chem. Appl.*, 2011, **525794**, 1–10.
55 P. O. Vardevanyan, A. P. Antonyan, M. A. Parsadanyan, H. G. Davtyan and A. T. Karapetyan, *Exp. Mol. Med.*, 2013, **35**, 527–533.
56 M. Ganeshpandian, R. Loganathan, E. Suresh, A. Riyasdeen, Md. A. Akbarsha and M. Palaniandavar, *Dalton Trans.*, 2014, **43**, 1203–1219.
57 V. Rajendiran, M. Murali, E. Suresh, S. Sinha, K. Somasundaram and M. Palaniandavar, *Dalton Trans.*, 2008, 148–163.
58 (*a*) C. Hiort, P. Lincoln and B. Norden, *J. Am. Chem. Soc.*, 1993, **115**, 3448–3454; (*b*) A. E. Friedman, J. C. Chamron, J. P. Sauvage, N. J. Turro and J. K. Barton, *J. Am. Chem. Soc.*, 1990, **112**, 4960–4962.
59 V. G. Sankareswari, D. Vinod, A. Mahalakshmi, M. Alamelu, G. Kumaresan, R. Ramaraj and S. Rajagopal, *Dalton Trans.*, 2014, **43**, 3260–3272.
60 S. S. Iqbal, M. W. Mayo, J. G. Bruno, B. V. Bronk, C. A. Battand and J. P. Chamber, *Biosens. Bioelectron.*, 2000, **15**, 549–578.
61 J. C. Pessoa and I. Tomaz, *Curr. Med. Chem.*, 2010, **17**, 3701–3738.
62 A. Levina, A. Mitra and P. A. Lay, *Metallomics*, 2009, **1**, 458–470.
63 H. Nagasawa, Y. Uto, K. L. Kirk and H. Hori, *Biol. Pharm. Bull.*, 2006, **29**, 2335.
64 J. Li, H. Chen, L. Zeng, T. W. Rees, K. Xiong, Y. Chen, L. Jia and H. Chao, *Inorg. Chem. Front.*, 2019, **6**, 1003–1010.
65 P. Liu, B. Wu, J. Liu, Y. Dai, Y. Wang and K. Wang, *Inorg. Chem.*, 2016, **55**, 1412–1422.
66 M. Sirajuddin, S. Ali and A. Badshah, *J. Photochem. Photobiol., B*, 2013, **124**, 1–19.
67 M. Shamsi-Sani, F. Shirini, M. Abedini and M. Seddighi, *Res. Chem. Intermed.*, 2016, **42**, 1091–1099.
68 S. Dasari and A. K. Patra, *Dalton Trans.*, 2015, **44**, 19844–19855.
69 J. Keizer, *J. Am. Chem. Soc.*, 1983, **105**, 1494–1498.
70 V. D. Suryawanshi, L. S. Walekar, A. H. Gore, P. V. Anbhule and G. B. Kolekar, *J. Pharm. Anal.*, 2016, **6**, 56–63.
71 K. Jeyalakshmi, J. Haribabu, C. Balachandran, S. Swaminathan, N. S. P. Bhuvanesh and R. Karvembu, *Organometallics*, 2019, **38**, 753–770.
72 S. Nikolić, L. Rangasamy, N. Gligorijević, S. Aranđelović, S. Radulović, G. Gasser and S. Grgurić-Šipka, *J. Inorg. Biochem.*, 2016, **160**, 156–165.

